Int. J. Solids Structures, 1977, Vol. 13, pp. 1019–1035. Pergamon Press. Printed in Great Britain

ELASTO-PLASTIC STRESS-STRAIN THEORY FOR COHESIONLESS SOIL WITH CURVED YIELD SURFACES

POUL V. LADE

Mechanics and Structures Department, School of Engineering and Applied Science, University of California, Los Angeles, CA 90024, U.S.A.

(*Received* 2 *August* 1976; *revised* 27 *January* 1977)

Abstract—An elasto-plastic stress-strain theory for cohesionless soil with curved yield surfaces is developed on the basis of soil behavior observed in laboratory tests. This theory is applicable to general three-dimensional stress conditions, but the parameters required to characterize the soil behavior can be derived entirely from results of isotropic compression and conventional drained triaxial compression tests. The theory is shown to predict soil behavior under various loading conditions with good accuracy. Of special interest is its capability of predicting soil behavior under drained as well as undrained conditions over a range of confining pressures where the behavior changes from that typical of dense sand to that typical of loose sand. Work-hardening as well as work-softening is incorporated in the theory.

1. INTRODUCTION

The elasto-plastic stress-strain theory previously developed for cohesionless soils[1, 2] reflects many of the characteristics of sand behavior observed in laboratory tests. Results of cubical triaxial tests on cohesionless soil[1, 3] and concepts from elasticity and plasticity were employed in formulating the theory, which incorporates a yield criterion, a non-associated flow rule, and an empirical work-hardening law.

This stress-strain theory is applicable to general three-dimensional conditions, but the values of the nine soil parameters required to characterize the soil behavior can be derived entirely from the results of conventional triaxial compression tests. Several essential aspects of the behavior of cohesionless soil observed in experimental investigations are modeled by the theory: nonlinearity, the influence of σ_2, stress-path dependency, shear-dilatancy effects, and coincidence of strain increment and stress increment axes at low stress levels with transition to coincidence of strain increment and stress axes at high stress levels. Results of cubical triaxial tests, torsion shear tests, and tests performed using various stress-paths were analyzed using this theory, and it was found that the stress-strain and strength characteristics observed in these tests were predicted with reasonable accuracy[1, 2, 4].

Involved in this theory are some simplifying assumptions, which result in limitations in its capabilities in some respects. Thus, only elastic strains are predicted for proportional loading[4], whereas laboratory tests show that proportional loading with increasing stresses causes some plastic deformation. Experiments show that failure envelopes for sands most often are curved in the Mohr diagram, whereas they are assumed to be straight in the previous theory. The gradual change in behavior characteristics with increasing confining pressure from those typical of dense sand to those typical of loose sand is not accounted for in the previously developed theory.

Incorporation of additional aspects of the real behavior of cohesionless soils in the stress-strain theory requires further development. The modified theory presented herein is based on the behavior observed in isotropic compression and triaxial compression tests on three different cohesionless soils, each tested at two different densities. All aspects of soil behavior included in the previous theory are retained, and the previous theory is merely a special case (i.e. for straight failure envelopes) which is contained within the framework of the new theory.

The accuracy of the theory presented here is evaluated by comparing predicted and measured strains for a number of laboratory test conditions. Thus, it is demonstrated that the theory can accurately predict soil behavior in triaxial tests over a range of confining pressures in which the maximum stress ratio decreases (curved failure envelope) and the volume change behavior becomes compressive with increasing confining pressure. The post-peak behavior is also correctly modeled in the range of confining pressures used in the tests. The predicted and

the measured behavior for proportional loading is compared, and "at rest" loading conditions can be calculated with good accuracy. Finally, pore pressures in undrained tests are predicted, and since stress-path dependency can be handled by the theory[4], most aspects of undrained behavior can be accounted for by the new theory.

2. BASIC BEHAVIOR OF COHESIONLESS SOILS

The development of the new theory is based on a consistent pattern of behavior observed from tests on three different cohesionless soils: Sacramento River Sand[5], Crushed Napa Basalt[6], and Painted Rock Material[7]. Each of the soils were tested at two different relative densities. These three soils had quite different characteristics in terms of composition, grain shape, grain size, and maximum and minimum void ratios. The diagrams used to illustrate the developments presented here refer to loose Sacramento River Sand (initial void ratio = 0.87, relative density = 38%).

2.1 *Types of strain*

For the purpose of modeling the stress-strain behavior of soils by an elasto-plastic theory, the total strain increments, $\{d\epsilon_{ij}\}$, are divided into an elastic component, $\{d\epsilon_{ij}^e\}$, a plastic collapse component, $\{d\epsilon_{ij}^c\}$, and a plastic expansive component, $\{d\epsilon_{ij}^p\}$, such that

$$\{d\epsilon_{ij}\} = \{d\epsilon_{ij}^e\} + \{d\epsilon_{ij}^c\} + \{d\epsilon_{ij}^p\}. \tag{1}$$

These strain components are calculated separately, the elastic strains by Hooke's law, the plastic collapse strains by a plastic stress-strain theory involving a cap-type yield surface, and the plastic expansive strains by a stress-strain theory which involves a conical yield surface with apex at the origin of the stress space.

Figure 1 illustrates schematically the parts of the total strain which for the present purpose are considered to be elastic, plastic collapse, and plastic expansive components of strain in a triaxial compression test. Typical observed variations of stress difference $(\sigma_1 - \sigma_3)$, and volumetric strain, ϵ_v, with axial strain, ϵ_1, are shown in this figure for a test performed with

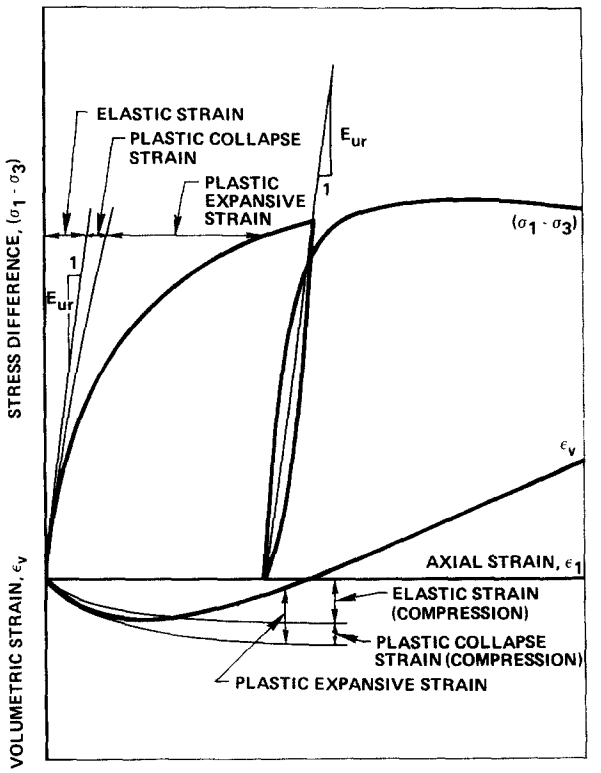

Fig. 1. Schematic illustration of elastic, plastic collapse and plastic expansive strain components in drained triaxial compression test.

constant value of the confining pressure, σ_3. Both elastic (recoverable) and plastic (irrecoverable) deformations occur from the beginning of loading of a cohesionless soil, the stress-strain relationship is nonlinear, and a decrease in strength follows peak failure. The volumetric strain is initially compressive and this behavior may be followed by expansion (as shown in Fig. 1) or by continued compression. The plastic strains are initially smaller than the elastic strains, but at higher values of stress difference the plastic strains dominate the elastic strains. The nature of the elastic, plastic collapse, and plastic expansive strain components and the methods of calculation for these components are discussed in the following.

3. ELASTIC STRAINS

The elastic strain increments, which are recoverable upon unloading, are calculated from Hooke's law, using the unloading-reloading modulus defined as[8]:

$$E_{ur} = K_{ur} \cdot p_a \cdot \left(\frac{\sigma_3}{p_a}\right)^n \tag{2}$$

The dimensionless, constant value of the modulus number K_{ur} and the exponent n are determined from triaxial compression tests performed with various values of the confining pressure, σ_3. In equation (2) p_a is atmospheric pressure expressed in the same units as E_{ur} and σ_3.

The value of Poisson's ratio has often been found to be close to 0.2 for the elastic parts of unloading-reloading stress-paths[8–10]. This value is therefore used in the following calculations.

4. PLASTIC COLLAPSE STRAINS

Part of the strains occurring during isotropic compression are irrecoverable, i.e. they are plastic in nature. Thus, a partial collapse of the grain structure resulting in a volumetric compression is caused by increasing isotropic stresses. This is illustrated in Fig. 2 for loose

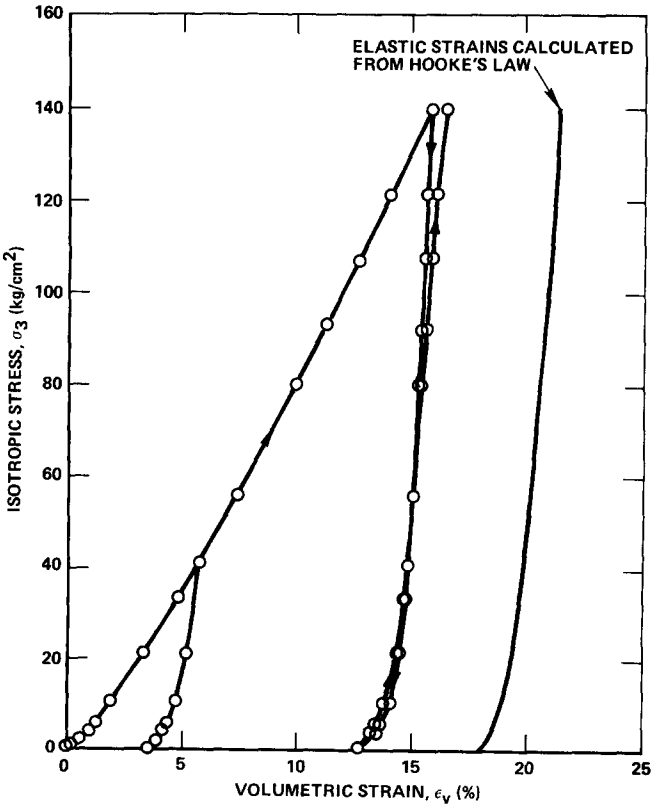

Fig. 2. Isotropic compression of loose Sacramento River Sand with primary loading, unloading and reloading branches.

Sacramento River Sand. The elastic strains which are recoverable upon unloading can be calculated with good accuracy from Hooke's law as shown in this figure. The collapse strains can therefore be separated from the total strains observed in these tests by subtracting the elastic strains.

It is reasonable to believe that plastic collapse strains are produced by any increase in mean normal stress, and that within this mode of behavior, plastic shear strains will be associated with shear stresses acting on the soil. However, it is difficult to separate the collapse strains from the plastic expansive strains for a general stress increment (not along the hydrostatic axis), because both types of strain occur simultaneously for such a stress increment. It is therefore necessary to find the magnitudes of the collapse strains from isotropic compression, the only loading condition which does not produce plastic expansive strains.

4.1 *Yield criterion.*

In order to model the described behavior, a yield criterion which forms a cap on the open end of the conical yield surface is used. Figure 3(a) shows the position of the yield cap. Cap-type yield criteria have been proposed in order to account for the plastic collapse strains occurring during isotropic compression[11–14]. Very often such cap yield surfaces have been continued smoothly into a conically shaped surface in such a way that the normality condition from theory of perfect plasticity[15, 16] could be employed over the entire surface[11, 12]. Two yield surfaces, a cone and a cap, have been used more recently[13, 14].

In the present development a collapse yield criterion which forms a sphere with center in the origin of the principal stress space is used in connection with the conical yield surface. The equation for the yield cap can be written in terms of the first and the second stress invariants, I_1 and I_2, as follows:

$$f_c = I_1^2 + 2 \cdot I_2 \tag{3}$$

As the value of f_c increases beyond its current value, the soil work-hardens and collapse strains are produced. It should be noted that yielding according to equation (3) does not result in eventual failure. Failure is controlled entirely by the conical yield surface.

4.2 *Plastic potential and flow rule*

Isotropic compression of an isotropic soil results in equal linear strains in the three principal directions. Thus, for this condition the strain increment vector should be pointed in the direction outward from the origin and coincide with the hydrostatic axis, as shown in Fig. 3(a). For this condition to be fulfilled the plastic potential function, g_c, must be identical to the yield criterion, f_c. The flow rule is then derived from:

$$\Delta\epsilon_{ij}^c = \Delta\lambda_c \cdot \frac{\partial f_c}{\partial \sigma_{ij}} \tag{4}$$

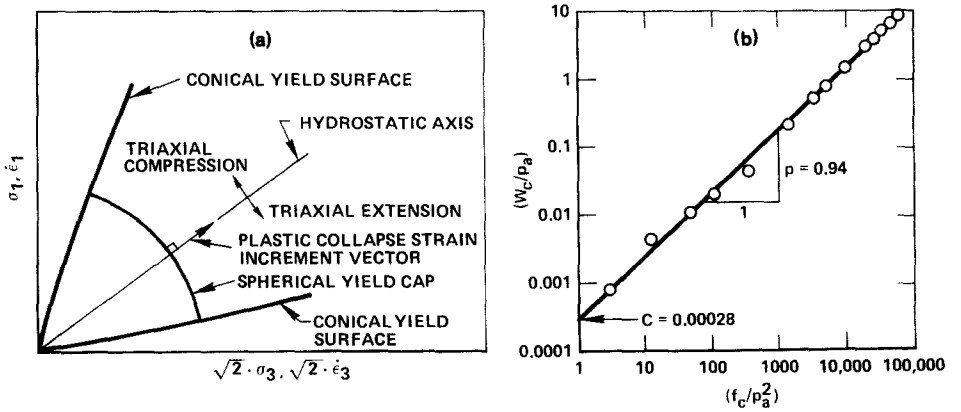

Fig. 3. (a) Location of yield cap relative to conical yield surface shown in triaxial plane, (b) relation between plastic collapse work, W_c, and the value of f_c for loose Sacramento River Sand.

where $\Delta\lambda_c$ is a proportionality constant. The derivatives of f_c with respect to the normal stresses become:

$$\frac{\partial f_c}{\partial \sigma_x} = 2 \cdot \sigma_x \tag{5a}$$

and similar expressions are obtained for the other normal stresses by interchanging the indices on the stresses. The derivatives of f_c with respect to the shear stresses become:

$$\frac{\partial f_c}{\partial \tau_{yz}} = 2 \cdot \tau_{yz} \tag{5b}$$

and similar expressions are obtained for the other shear stresses by interchanging the indices on the stresses.

4.3 *Work-hardening law*

The collapse stress-strain relationship involves one parameter, $\Delta\lambda_c$, which determines the absolute magnitude of the strain increment. The value of $\Delta\lambda_c$ can be determined from the work-hardening law.

The magnitudes of the strain increments can be calculated using an experimentally determined relation between the total plastic work required to produce collapse strains, W_c, and the degree of hardening expressed by f_c (from eqn 3):

$$W_c = F_c(f_c) \tag{6}$$

where F_c is a monotonically increasing, positive function. It is assumed that the relation expressed in eqn (6) is unique, and this implies that the work-hardening relationship is independent of the stress-path.

The relationship expressed in eqn (6) can be determined empirically from an isotropic compression test. The plastic work is calculated from

$$W_c = \int \{\sigma_{ij}\}^T \{d\epsilon_{ij}^c\} \tag{7}$$

which for isotropic compression reduces to

$$W_c = \int \sigma_3 \cdot d\epsilon_v^c \tag{8}$$

where $\sigma_3 \cdot d\epsilon_v^c$ is the plastic work done per unit volume during the volumetric strain increment $d\epsilon_v^c$.

The value of f_c reduces for isotropic compression to

$$f_c = 3 \cdot \sigma_3^2. \tag{9}$$

The diagram in Fig. 3(b) shows the relationship between W_c and f_c plotted on log-log scales for loose Sacremento River Sand. This relationship can be described with good accuracy as a straight line for which the following expression is used

$$W_c = C \cdot p_a \cdot \left(\frac{f_c}{p_a^2}\right)^p. \tag{10}$$

The dimensionless, constant value of the collapse modulus C is determined at $f_c/p_a^2 = 1$ and the collapse exponent p is the slope of the straight line as indicated in Fig. 3(b). In eqn (10) p_a is atmospheric pressure expressed in the same units as W_c and $\sqrt{f_c}$.

Noting that the yield criterion in eqn (3) is a homogeneous function of degree 2 and following

the development outlined in[17], the proportionality constant $\Delta\lambda_c$ in eqn (4) can be written as:

$$\Delta\lambda_c = \frac{dW_c}{2 \cdot f_c} \tag{11}$$

where dW_c is the increment in plastic collapse work over the increment $df_c(\geq 0)$. The value of dW_c may be determined from the derivative of W_c (given in eqn 10) with regard to (f_c/p_a^2):

$$dW_c = C \cdot p \cdot p_a \cdot \left(\frac{p_a^2}{f_c}\right)^{1-p} \cdot d(f_c/p_a^2). \tag{12}$$

The plastic collapse stress-strain relations are then determined from eqns (4), (5), (11) and (12).

5. PLASTIC EXPANSIVE STRAINS

The component of strain which has been referred to as plastic and expansive is shown in Fig. 1. Experimental evidence suggests, however, that some compression occurs due to shear stresses at small stress levels before the plastic strains become expansive at higher stress levels[18, 19]. Although compression is included, the component of strain dealt with in this section will be referred to as plastic expansive strain.

5.1 *Failure criterion–failure surface*

The failure surface is curved for most cohesionless soils, i.e. the friction angle decreases with increasing magnitude of the mean normal stress. In order to include this curvature in the failure criterion, data from triaxial compression tests on many different cohesionless soils were studied. A suitable relationship between the stresses at failure was developed in terms of the first and the third stress invariants, I_1 and I_3:

$$f_p = (I_1^3/I_3 - 27) \cdot (I_1/p_a)^m \tag{13a}$$

$$f_p = \eta_1 \text{ at failure} . \tag{13b}$$

The values of η_1 and m in eqn (13) can be determined by plotting $(I_1^3/I_3–27)$ vs (p_a/I_1) at failure in a log–log diagram, as shown in Fig. 4 for loose Sacramento River Sand. On this diagram η_1 is the intercept with $(p_a/I_1) = 1$ and m is the slope of the straight line.

In principal stress space the failure surface defined by eqn (13) is shaped like an asymmetric bullet with the pointed apex at the origin of the stress space as shown in Fig. 5(a). The apex angle increases with the value of η_1, and the curvature of the failure surface increases with the value of m. For $m = 0$ the failure surface is straight and the expression in eqn (13) becomes identical to that used in the previous theory[1, 2]. Figure 5(b) shows typical cross-sections for given values of I_1^3/I_3 and for constant value of I_1. These cross-sections are exactly the same as for the previous

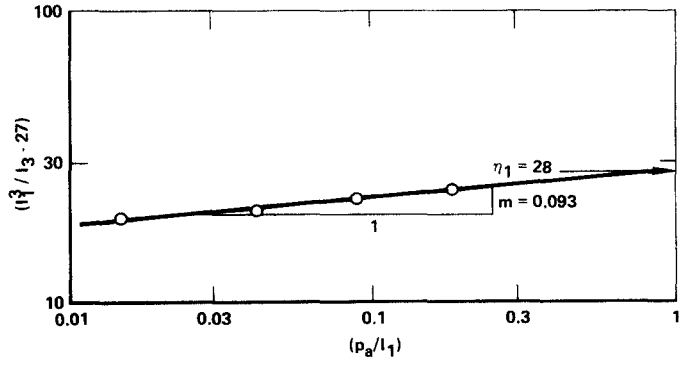

Fig. 4. Determination of the values of η_1 and m involved in failure criterion for loose Sacramento River Sand.

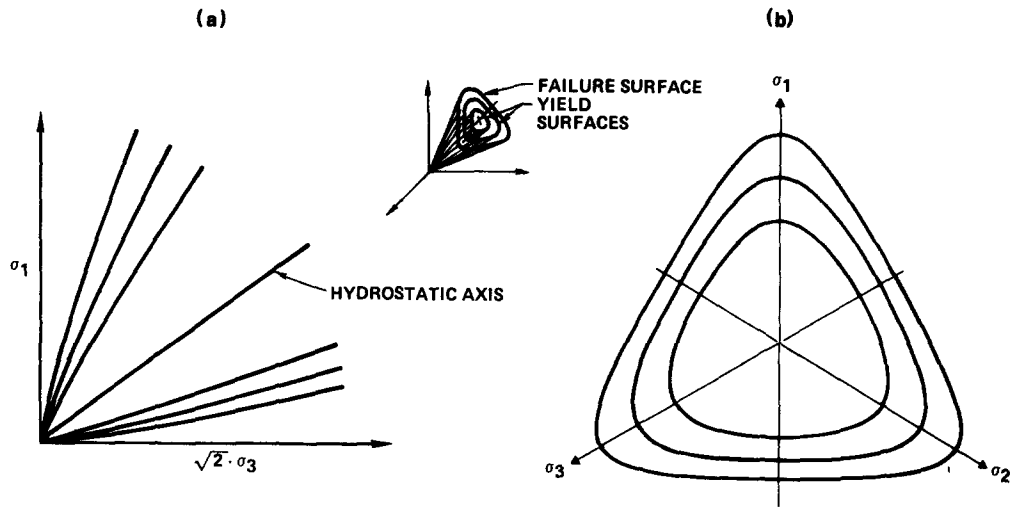

Fig. 5. Characteristics of proposed failure and yield surfaces shown in principal stress space. (a) Traces of failure and yield surfaces in triaxial plane. (b) Traces of failure and yield surfaces in octahedral plane.

theory, and it has been shown that they model the experimentally determined three-dimensional strengths of sands with good accuracy[1, 2].

The failure surface given in eqn (13) is always concave towards the hydrostatic axis. However, the real failure surfaces for cohesionless soils open up and become conical at very high values of the mean normal stress[5]. The failure criterion is therefore only valid in the range of mean normal stresses where the failure surface is concave towards the hydrostatic axis. This range of mean normal stresses is dependent on the integrity of the soil grains, and only when crushing becomes an important factor in the soil behavior does the real failure surface deviate from that expressed in eqn (13). However, for most soils the stresses necessary to produce appreciable crushing are of a magnitude to be found, e.g. at the bottom of very tall earth dams.

5.2 *Yield surface-yield criterion*

The yield surface, which defines the boundary between states of stress where both elastic and plastic deformations occur and those where only elastic deformations occur, is assumed to have the same general shape as the failure surface and to be expressible by eqn (13a). During continued loading the yield surface expands symmetrically around the hydrostatic axis as the value of f_p increases, such as shown in the insert in Fig. 5. The ultimate position of the yield surface for which $f_p = \eta_1$ is the failure surface for the sand. During unloading and neutral loading, the yield surface remains in the same position corresponding to the highest value of f_p previously applied to the sand. Thus, the soil is assumed to harden isotropically.

5.3 *Plastic potential and flow rule*

It is often assumed in plasticity theory that the plastic potential and the yield criterion are identical. This assumption was employed for the behavior of the plastic collapse strains. However, it has been found that this assumption is not accurate for the plastic expansive strain component[3, 4, 20, 21]. The plastic potential function incorporated in the theory described herein is expressed in a form similar to the failure criterion:

$$g_p = I_1^3 - \left(27 + \eta_2 \cdot \left(\frac{p_a}{I_1}\right)^m\right) \cdot I_3 \tag{14}$$

where η_2 is a constant for given values of f_p and σ_3. The plastic potential function describes a series of surfaces which are normal to the plastic strain increment directions. The selection of the function in eqn (14) was based on observations made during this and previous studies[1–4] of the directions of plastic strain increments determined from experiments.

The plastic potential surfaces given by eqn (14) are shaped like asymmetric bullets with

their pointed apices at the origin of the stress space. Their traces in octahedral planes are the same as those for the yield surfaces (Fig. 5b). Their traces in triaxial planes resemble those of the yield surface (Fig. 5a), but their apex angles are greater, they are more curved, they cut the yield surfaces, and they become asymptotic to the hydrostatic axis at a greater rate than the yield surfaces.

The relation between stress and strain is derived according to the following expression:

$$\Delta\epsilon_{ij}^{p} = \Delta\lambda_p \cdot \frac{\partial g_p}{\partial \sigma_{ij}} \tag{15}$$

which expresses that the strain increments are proportional to the derivatives of the plastic potential. The derivatives of g_p with respect to the normal stresses become:

$$\frac{\partial g_p}{\partial \sigma_x} = 3 \cdot I_1^2 - \left(27 + \eta_2 \cdot \left(\frac{p_a}{I_1}\right)^m\right) \cdot \left(\sigma_y \cdot \sigma_z - \tau_{yz}^2\right) + \frac{I_3}{I_1} \cdot m \cdot \eta_2 \cdot \left(\frac{p_a}{I_1}\right)^m$$

and similar expressions are obtained for the other normal stresses by interchanging the indices on the stresses. The derivatives of g_p with respect to the shear stresses become:

$$\frac{\partial g_p}{\partial \tau_{yz}} = \left(27 + \eta_2 \cdot \left(\frac{p_a}{I_1}\right)^m\right) \cdot (\sigma_x \cdot \tau_{yz} - \tau_{xy} \cdot \tau_{zx}) \tag{16b}$$

and similar expressions are obtained for the other shear stresses by interchanging the indices on the stresses.

A significant feature of the stress-strain relations is that they model the coupling between shear stresses and normal strains (eqns 15 and 16a) and between normal stresses and shear strains (eqns 15 and 16b). These coupling effects are consistent with observed soil behavior.

Two parameters are involved in the stress-strain relationship: $\Delta\lambda_p$ and η_2. The value of $\Delta\lambda_p$ determines the magnitude of the plastic strain increment, and the value of η_2 determines the directions of the strain increments in planes perpendicular to the octahedral plane.

The value of η_2 may be determined from the directions of the plastic strain increments in the triaxial plane, as shown for the similar strain increment directions in connection with the previous theory [1, 2]. η_2 can be determined by expressing:

$$\nu^p = -\frac{\Delta\epsilon_3^{\,p}}{\Delta\epsilon_1^{\,p}} \tag{17}$$

Substituting expressions for $\Delta\epsilon_1^{\,p}$ and $\Delta\epsilon_3^{\,p}$ from eqns (15) and (16a) into eqn (17) and solving for η_2 gives:

$$\eta_2 = \frac{3 \cdot (1 + \nu^p) \cdot I_1^2 - 27 \cdot \sigma_3 \cdot (\sigma_1 + \nu^p \cdot \sigma_3)}{\left(\frac{p_a}{I_1}\right)^m \cdot \left[\sigma_3 \cdot (\sigma_1 + \nu^p \cdot \sigma_3) - \frac{m \cdot (1 + \nu^p) \cdot I_1^2}{f_p \cdot (p_a/I_1)^m + 27}\right]} \cdot \tag{18}$$

It is assumed that the values of η_2 calculated from the triaxial compression tests at any stress level are the correct values to use for prediction of the relative magnitudes of the strain increments at the same stress levels in tests with any combination of the three principal stresses. This assumption was shown to result in good agreement between observed behavior and the predictions of the previous theory [1, 2].

Values of η_2 were calculated from eqn (18) and plotted as a function of f_p given by eqn (13a). In order to determine the ratio $\nu^p = -\Delta\epsilon_3^{\,p}/\Delta\epsilon_1^{\,p}$ from the triaxial compression tests, the plastic expansive strain increments were calculated by subtracting the elastic and the plastic collapse strains from the total strains according to eqn (1). The variation of η_2 with f_p and σ_3 is shown in Fig. 6(a) for loose Sacramento River Sand. It may be seen from this figure that η_2 is very nearly linearly related to f_p for constant values of σ_3. The slopes of the straight lines are the same, but the intercept of the lines with the η_2-axis vary with σ_3. The variation of η_2 can be

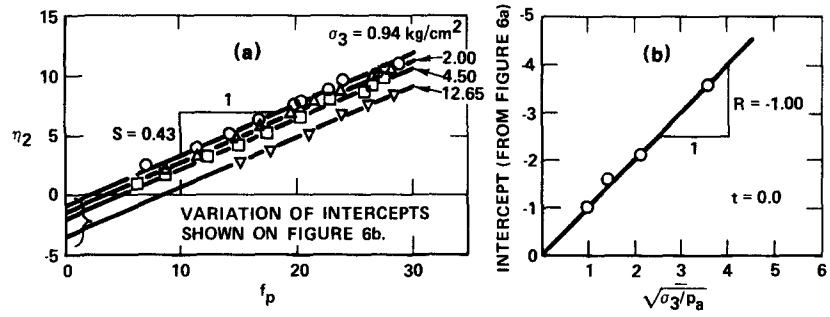

Fig. 6. (a) Variation of η_2 with f_c and σ_3. (b) Variation of intercepts with σ_3 for loose Sacramento River Sand.

modeled by a simple expression of the following type:

$$\eta_2 = S \cdot f_p + R \cdot \sqrt{\frac{\sigma_3}{p_a}} + t \tag{19}$$

where S is the slope of the straight lines, and the last two terms model the variation of the intercept. R and t are constants to be determined as shown on the diagram in Fig. 6(b).

Considerations of the strain increment ratios suggest that the value of η_2 should be zero for isotropic stress conditions where the value of f_p is also zero. However, the plastic strains which occur for very small values of f_p are negligible, and the fact that the straight lines, which model the variations of η_2, do not go through the origin is therefore not of practical importance.

Negative values of η_2 correspond to plastic volumetric strains which are compressive, whereas positive values of η_2 correspond to plastic expansive strains. Figure 6(a) shows that loose Sacremento River Sand compresses slightly at small stress levels before expansive strains are produced at high stress levels. The diagram indicates that the initial compression is most pronounced for high confining pressures, which is in accordance with observed soil behavior.

The experimental data show that the values of η_2 are smaller than f_p, thus indicating that the plastic potential surface and the yield surface do not coincide. If η_2 was equal to f_p at all stress levels, the plastic potential function in eqn (14) would be identical to the yield function in eqn (13a) and the normality criterion would apply to the soil. However, Fig. 6(a) indicates that the chosen yield criterion cannot substitute as the plastic potential function for cohesionless soil.

5.4 *Work-hardening and -softening law*

The magnitudes of the strain increments caused by a given stress increment can be calculated using an experimentally determined relation between plastic work and stress level. An isotropic work-hardening and -softening law is employed, and this implies that the yield surface expands or contracts uniformly and that the degree of hardening or softening is independent of stress-path. Thus, according to the isotropic hardening hypothesis, there exists a unique relationship between the total plastic work W_p and the degree of hardening or softening expressed by the value of f_p (given by eqn 13a):

$$W_p = F_p(f_p) \tag{20}$$

where F_p is a monotonically increasing or decreasing, positive function.

The relationship expressed in eqn (20) can be determined empirically by calculating the plastic work and plotting its variation with f_p. The plastic work at each stage of the triaxial compression tests was calculated from

$$W_p = \int \{\sigma_{ij}\}^T \{d\epsilon_{ij}^p\} \tag{21}$$

in which $\{\sigma_{ij}\}^T\{d\epsilon_{ij}^p\}$ is the plastic work done per unit volume during the strain increment $\{d\epsilon_{ij}^p\}$. The diagram in Fig. 7 shows the variation of the total plastic work with the value of f_p and the

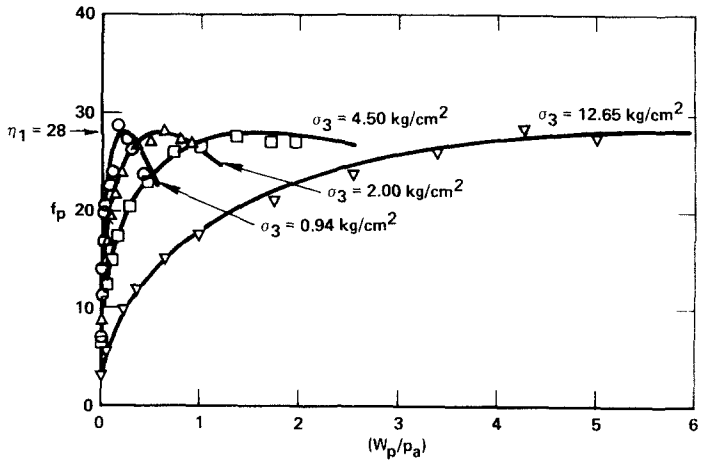

Fig. 7. Variation of total plastic work with f_p and σ_3 for loose Sacramento River Sand.

confining pressure σ_3. The fact that very small or negligible plastic strains are produced at small stress levels (as shown schematically in Fig. 1) is reflected in the work-hardening relationships which have vertical tangents at the origin. Increasing increments of plastic strains are produced with increasing stress levels. Figure 7 also demonstrates a significant influence of the confining pressure on the amount of plastic work necessary to produce plastic strains at high stress levels. The peaks of the relationships all occur at $f_p = \eta_1$, but the amount of plastic work required to reach the peaks increases with increasing confining pressure. The decreases in the values of f_p with further work input also follow a consistent pattern which depends on σ_3, as shown in Figure 7. This post-peak behavior is referred to as work-softening or strain softening.

In order to be able to handle both work-hardening and work-softening, it is necessary to consider the function F_p in eqn (20) first as monotonically increasing and then as monotonically decreasing. Therefore, the value of W_p at the peak stress level (i.e. at peak failure) is used to distinguish between the parts of the relation between W_p and f_p where F_p is increasing and the parts where F_p is decreasing.

The plastic potential function for the plastic expansive strains (eqn 14) is not a homogeneous function. However, proceeding as in [17], the operations indicated in the expression $\sigma_{ij} \cdot (\partial g_p / \partial \sigma_{ij})$ result in

$$\sigma_{ij} \cdot \frac{\partial g_p}{\partial \sigma_{ij}} = 3 \cdot g_p + m \cdot \eta_2 \cdot \left(\frac{p_a}{I_1}\right)^m \cdot I_3. \tag{22}$$

The value of the proportionality constant $\Delta\lambda_p$ in eqn (15) can therefore be written as

$$\Delta\lambda_p = \frac{dW_p}{3 \cdot g_p + m \cdot \eta_2 \cdot \left(\frac{p_a}{I_1}\right)^m \cdot I_3} \tag{23}$$

where g_p is the plastic potential function and dW_p is the increment in plastic work due to an increase in the stress level df_p.

The increment of plastic work per volume, dW_p, can be determined from the relations between W_p and f_p shown in Fig. 7. These rlations can be approximated by exponential functions for which the following expression is used:

$$f_p = a \cdot e^{-b \cdot W_p} \cdot \left(\frac{W_p}{p_a}\right)^{1/q}, \quad q > 0 \tag{24}$$

where the parameters a, b and q are constants for a given value of the confining pressure σ_3.

The expression in eqn (24) models several aspects of the work-hardening and work-softening behavior shown in Fig. 7: (1) The initial tangent is vertical, and the expression

therefore models the soil behavior at the origin, as discussed above; (2) the value of f_p increases with W_p until a peak value is reached; and (3) f_p decreases with further increase in W_p in a way similar to that exhibited by the soil behavior. The only limitiation of the exponential expression in eqn (24) is that the value of f_p decreases asymptotically to zero for very large values of W_p. Thus, it implies that the residual strength of the soil is zero. However, eqn (24) models the soil behavior very accurately within strain magnitudes of interest, and only for very large strains does it deviate from the observed soil behavior.

The values of q, a and b in eqn (24) can be determined for a given value of the confining pressure according to the following expressions:

$$q = \frac{\log\left(\frac{W_{ppeak}}{W_{p60}}\right) - \left(1 - \frac{W_{p60}}{W_{ppeak}}\right) \cdot \log e}{\log\left(\frac{\eta_1}{f_{p60}}\right)} \tag{25}$$

where (W_{p60}, f_{p60}) and (W_{ppeak}, η_1) are two sets of corresponding values on a curve in Fig. 7 and e is the base for natural logarithms. Any two points on a curve could in principle be used for determination of q, but the best overall curvefit is obtained when the peak point of the curve and the point corresponding to 60% of η_1 on the work-hardening part of the curve are used.

$$a = \eta_1 \cdot \left(\frac{e \cdot p_a}{W_{ppeak}}\right)^{1/q} \tag{26}$$

and

$$b = \frac{1}{q \cdot W_{ppeak}} \tag{27}$$

where q is determined from eqn (25), e is the base for natural logarithms and W_{ppeak} is the value of W_p at the peak point.

The variation of W_{ppeak} with the confining pressure σ_3 is shown on the diagram in Fig. 8(a), and this variation can be approximated by a straight line in the log–log diagram, such that

$$W_{ppeak} = P \cdot p_a \cdot \left(\frac{\sigma_3}{p_a}\right)^l \tag{28}$$

where P and l are constants to be determined as shown on Fig. 8(a) and p_a is atmospheric pressure expressed in the same units as W_{ppeak} and σ_3.

The variation of q with confining pressure σ_3 is shown on the diagram in Fig. 8(b), and this variation can best be modeled by a simple expression as follows:

$$q = \alpha + \beta \cdot \frac{\sigma_3}{p_a} \tag{29}$$

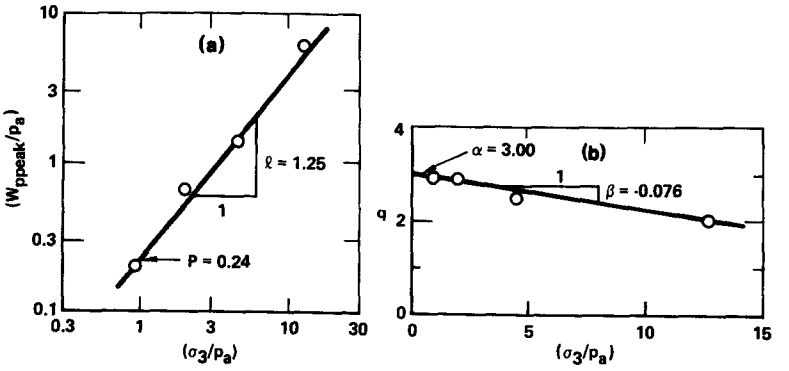

Fig. 8. (a) Variation of W_{ppeak} with confining pressure σ_3 and (b) variation of q with confining pressure σ_3 for loose Sacramento River Sand.

where α and β are, respectively, the intercept and the slope of the straight line shown on Fig. 8(b).

The solid lines on Fig. 7 have been drawn on the basis of the relationship in eqn (24) and the values of a, b, and q determined from eqns (26)–(29). It may be seen that the expression in eqn (24) models all aspects of the observed soil behavior with good accuracy for all values of the confining pressure σ_3.

Based on the expression in eqn (24) the increment in plastic work can be expressed as follows:

$$dW_p = \frac{df_p}{f_p} \cdot \frac{1}{\left(\frac{1}{q \cdot W_p} - b\right)} \tag{30}$$

where q is given by eqn (29), b is given by eqns (27) and (28), f_p is the current value of the stress level, and df_p is the difference in f_p between two successive stress states.

It should be noted that it is important to distinguish between the work-hardening and the work-softening parts of the $W_p - f_p$ relationship, because two values of W_p corresponds to the same value of f_p. This is best done by comparing the current value of W_p with W_{ppeak} calculated from eqn (28). Thus, for $W_p < W_{ppeak}$ the soil is work-hardening and for $W_p > W_{ppeak}$ the soil is work-softening. For $W_p = W_{ppeak}$ the value of dW_p in eqn (30) is infinite. For all other conditions the value of dW_p is positive and definite. The calculations presented in Section 7 were made on the basis of total stresses rather than stress increments, and the condition $W_p = W_{ppeak}$ could therefore easily be avoided with no loss in accuracy.

6. SUMMARY OF STRESS-STRAIN PARAMETERS

The values of the parameters included in the elasto-plastic stress-strain theory presented above can be evaluated using only the results of isotropic compression and conventional drained triaxial compression tests. The values of the parameters were determined from the results of tests on Sacramento River Sand, Crushed Napa Basalt, and Painted Rock Material, each tested at two different relative densities. The parameters are listed in Table 1. It should be noted that none of these parameters have dimensions. All dimensions are controlled, where appropriate, by the dimension of the atmospheric pressure, p_a, as e.g. in eqn (28). The parameters in Table 1 may be used to calculate strains in the respective soils for any combination of stresses and changes in stress during primary loading, neutral loading, unloading, and reloading.

Table 1. Summary of soil parameters for Sacramento River Sand, crushed Napa basalt, and painted rock material

Parameter \ Soil	Sacramento River Sand		Crushed Napa Basalt		Painted Rock Material		Strain Component
Relative Density, D_r(%)	100	38	100	70	100	70	
Void Ratio, e	0.61	0.87	0.53	0.66	0.40	0.48	
Modulus No., K_{ur}	1680	960	1520	900	1580	730	Elastic
Exponent, n	0.57	0.57	0.34	0.38	0.49	0.66	
Poisson's Ratio, ν	0.20	0.20	0.20	0.20	0.20	0.20	
Collapse Modulus, C	0.00023	0.00028	0.00075	0.00120	0.00100	0.00140	Plastic Collapse
Collapse Exponent, p	0.86	0.94	0.74	0.775	0.63	0.644	
Yield Const., η_1	80	28	280	130	101	67	
Yield Exponent, m	0.23	0.093	0.423	0.30	0.21	0.16	
Pl. Potent. Const., R	-2.95	-1.00	-5.90	-3.03	-2.34	-2.21	
Pl. Potent. Const., S	0.44	0.43	0.41	0.40	0.44	0.44	Plastic
Pl. Potent. Const., t	8.45	0.00	0.00	0.00	2.80	3.10	Expansive
Work-Hard. Const., α	3.00	3.00	2.22	2.35	3.45	3.28	
Work-Hard. Const., β	0.060	-0.076	-0.023	-0.046	-0.033	-0.029	
Work-Hard. Const., P	0.12	0.24	0.50	0.35	0.12	0.080	
Work-Hard. Exponent, ℓ	1.16	1.25	1.09	1.23	1.38	1.61	

7. PREDICTION OF SOIL BEHAVIOR FOR VARIOUS LOADING CONDITIONS

To test the abilities of the elasto-plastic stress-strain theory developed in the previous sections, predictions of this theory are compared to measured soil behavior for a variety of loading conditions. In addition to results of drained triaxial compression tests, experimental data are available for proportional loading and undrained compression on Sacramento River Sand and for "at rest" loading conditions on Crushed Napa Basalt and Painted Rock Material. These types of loading conditions are of special interest because they were either predicted with only moderate accuracy or they were not compared to the predictions of the previous theory. Appropriate computer programs were developed to perform the necessary calculations involved in using the theory for prediction of the various loading conditions. Only the soil parameters listed in Table 1 are used for all predictions.

7.1 *Drained triaxial compression tests*

The relation between stress difference, volumetric strain, and axial strain for drained triaxial compression tests were determined by specifying discrete stress points for such tests and calculating the strain increments from the theory. The comparison between measured and calculated stress-strain and volume change behavior for loose and dense Sacramento River Sand is shown in Fig. 9. The points in these figures represent the measured soil behavior and the solid lines represent the calculations from the theory.

Most aspects of the soil behavior are calculated with good accuracy using the stress-strain theory. Notably, the decrease in maximum stress ratio, σ_1/σ_3, with increasing confining pressure is well accounted for, and the gradual variation of the volumetric strain behavior, from being expansive at small confining pressures to being compressive at high confining pressures, is also modeled correctly by the theory. The predicted post-peak stress-strain curves are in good agreement with those measured within the range of strains considered.

7.2 *Proportional loading*

Proportional loading is defined as a loading condition where the ratio between the principal stresses is held constant while the stress magnitudes are increased or decreased. Tests with proportional loading and decreasing stresses result in only elastic strains [4, 22, 23]. Proportional loading with increasing stresses results in both elastic and plastic strains, and the measured

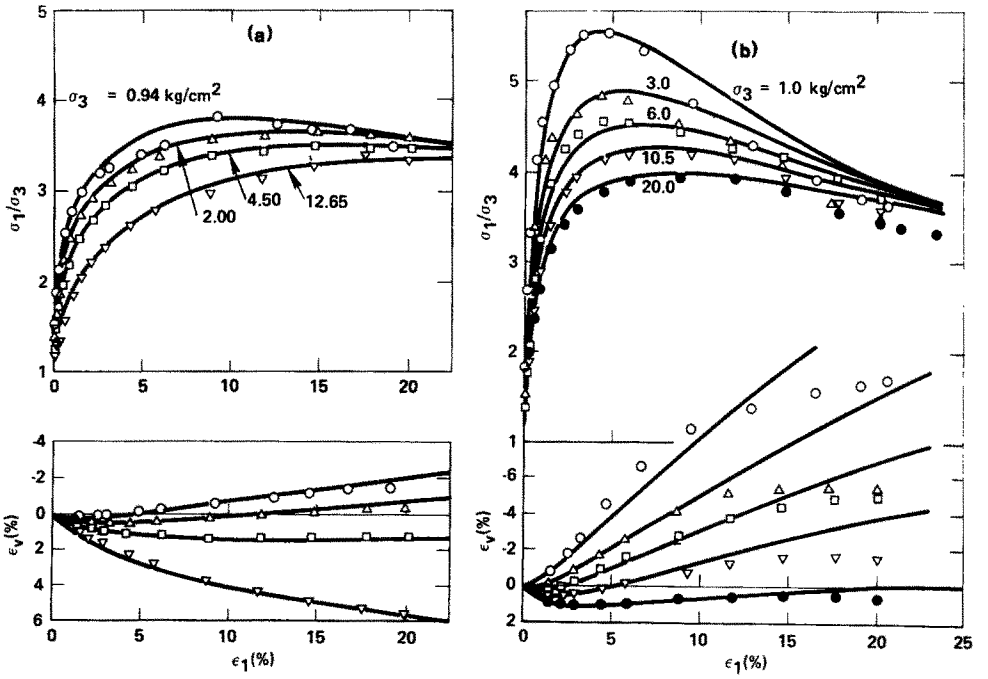

Fig. 9. Comparison between measured and predicted stress-strain and volume change behavior for (a) loose and (b) dense Sacramento River Sand in drained triaxial compression tests.

axial and volumetric strains generally become larger with increasing stress ratio [4, 9, 22, 23].

Curved yield surfaces are used for the plastic expansive strains, and both yield surfaces, the cone and the cap, are therefore pushed out when the stresses are increased proportionally. Thus, both elastic and plastic strains will occur for proportional loading with increasing stresses. Only elastic strains are predicted by the theory for conditions of constant stress ratio and decreasing stresses, which is in accordance with observed soil behavior [4].

Prediction of stress-strain relations for proportional loading were performed by specifying discrete stress points and calculating the strain increments from the theory. Figure 10 shows observed and predicted strains for proportional loading conditions with increasing stresses on loose and dense Sacramento River Sand. Stress ratios of 1.00, 1.77, 2.20 and 2.80 were used in the tests. Figure 10(a) shows that the axial strains for the loose sand are calculated to be somewhat higher (solid lines) than those measured (points). However, the volumetric strains are fairly accurately predicted for all values of the stress ratio. Figure 10(b) shows that both axial and volumetric strains for the dense sand are predicted with good accuracy for all stress ratios. The volumetric compression of the dense sand is quite similar in magnitude for all stress ratios used, whereas the loose sand shows increasing volumetric compression with increasing stress ratio. This difference in behavior is predicted by the theory.

7.3 *"At rest" loading conditions*

Tests performed on specimens under conditions of zero lateral strain are referred to as "at rest" tests or K_o-tests, where K_o is the coefficient of earth pressure at rest which may be defined as [24]:

$$K_o = \left(\frac{\Delta\sigma_3}{\Delta\sigma_1}\right)_{\epsilon_h=0} \tag{31}$$

where $\Delta\sigma_3$ and $\Delta\sigma_1$ are the increments in the principal stresses such that no lateral strain occurs. For the case of increasing stresses both plastic and elastic strains are produced, whereas mainly elastic strains occur in the specimen for the case of decreasing stresses [24]. For increasing stresses the plastic and the elastic strains cancel each other out such that the total lateral strain is zero:

$$\Delta\epsilon_h{}^e + \Delta\epsilon_h{}^c + \Delta\epsilon_h{}^p = 0 \tag{32}$$

where $\Delta\epsilon_h{}^e$, $\Delta\epsilon_h{}^c$, and $\Delta\epsilon_h{}^p$ refer to lateral increments in elastic, plastic collapse, and plastic expansive strains.

The soil behavior during K_o-tests was calculated by specifying the vertical stresses and using a simple iteration procedure to find the horizontal stresses that would result in lateral strains fulfilling eqn (32) within specified narrow limits. The results of a K_o-test on dense Crushed Napa Basalt (relative density = 100%) are shown on Fig. 11. The predicted behavior

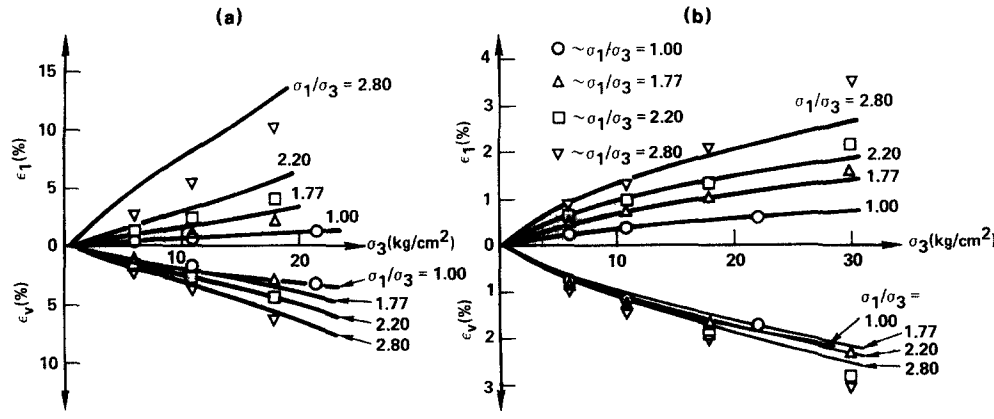

Fig. 10. Comparison of measured and predicted strains for proportional loading with increasing stresses on (a) loose and (b) dense Sacramento River Sand.

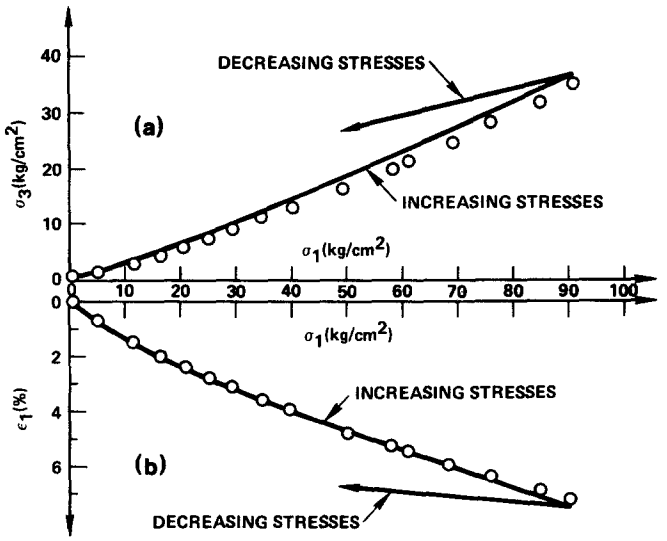

Fig. 11. Comparison of measured and predicted (a) stresses and (b) stress-strain relationship in K_o-test on dense crushed Napa basalt.

(solid lines) is seen to correspond very well to the measured behavior (points) for increasing stresses. The value of K_o calculated from eqn (3) is not constant as is often assumed. K_o increases with increasing stresses, and this aspect of the soil behavior is accurately predicted by the theory. No test results were available for decreasing stresses, but tests by others[25–27] indicate that they follow a pattern shown by the lines denoted "Decreasing Stresses." The states of stress and the axial strains indicated by these lines are actually the ones predicted by the theory. The value of K_o for decreasing stresses may be calculated from elasticity theory and corresponds to $K_o = \nu/(1-\nu)$, where $\nu = 0.2$ is Poisson's ratio.

7.4 *Undrained triaxial compression tests*

The prediction of pore pressures and soil behavior in undrained tests on saturated specimens is based on the condition that no volume change occurs in the soil for any load increment:

$$\Delta\epsilon_v^e + \Delta\epsilon_v^c + \Delta\epsilon_v^p = 0 \tag{33}$$

where $\Delta\epsilon_v^e$, $\Delta\epsilon_v^c$ and $\Delta\epsilon_v^p$ are the volumetric strain components corresponding to the three types of strain occurring in the soil. The calculation of pore pressures was performed by specifying the chamber pressure and discrete values of effective stress ratio, σ_1'/σ_3', or stress difference, $(\sigma_1 - \sigma_3)$. The effective confining pressure producing volumetric strains which would satisfy eqn (33) within specified limits was found by iteration. The pore pressure was then calculated as the difference between the chamber pressure and the required effective confining pressure. It should be noted that calculation of pore pressures and soil behavior using the restraint in eqn (33) is based on the fact that a balance can be found between the compressive volumetric strains, $\Delta\epsilon_v^e$ and $\Delta\epsilon_v^c$, and the expansive volumetric strains, $\Delta\epsilon_v^p$, such that their sum is zero at each stress level.

The results of isotropically consolidated undrained triaxial compression tests were available for loose and dense Sacramento River Sand[28], and these results were used for comparison with the predictions of the theory. Two examples which illustrate the capabilities of the theory are shown in Fig. 12. The test on loose sand was performed with an initial effective confining pressure of 12.65 kg/cm^2. Figure 12(a) shows that the variation of both the effective stress ratio, σ_1'/σ_3', and the pore pressure, u, with axial strain is correctly predicted. The initial effective confining pressure for the test on dense sand was 10.50 kg/cm^2 as shown in Fig. 12(b). After the initial increase, the pore pressure decreased to -0.9 kg/cm^2 at which cavitation of the pore water was observed. After cavitation was initiated, the specimen expanded as in a conventional drained test. The fact that cavitation occurred at -0.9 kg/cm^2 was included in the calculations.

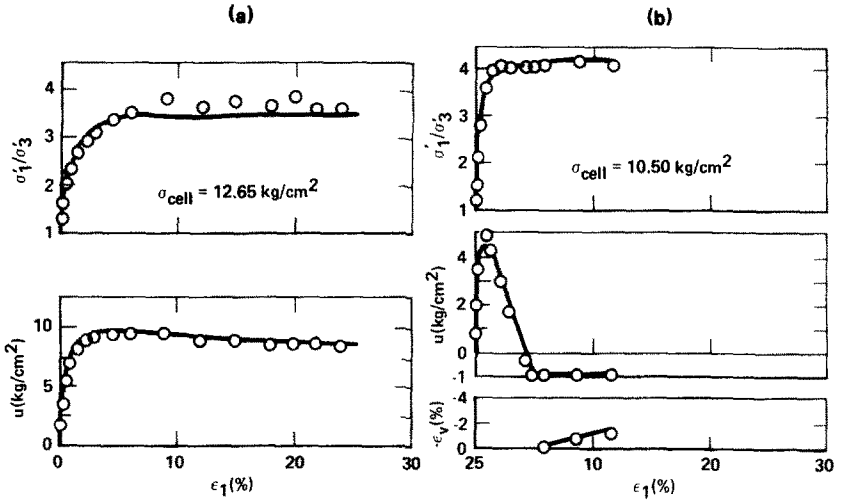

Fig. 12. Comparison of measured and predicted stress-strain, pore pressure, and volume change behavior for undrained tests on (a) loose and (b) dense Sacramento River Sand.

The observed stress-strain, pore pressure, and volume change behavior in the undrained test on dense sand is also predicted accurately by the theory presented herein.

8. SUMMARY AND CONCLUSIONS

An elasto-plastic stress-strain theory for cohesionless soil with curved yield surfaces has been developed on the basis of the soil behavior observed in isotropic compression and triaxial compression tests performed on three different cohesionless soils, each tested at two different relative densities. This development constitutes an expansion of a previously presented stress-strain model such that additional aspects of soil behavior could be incorporated in the theoretical framework. The yield criterion, the plastic potential, and the work-hardening law included in the constitutive law presented here have all been modified relative to those used in the previous theory. In addition, work-softening is included in the new theory, and the irrecoverable strains which occur during isotropic compression are modeled by a separate plasticity theory which involves a cap-type yield surface.

The accuracy of the modified theory has been evaluated by comparing predicted and measured strains for several types of laboratory tests performed on loose and dense sand. Thus, it is demonstrated that the modified theory can accurately predict soil behavior in triaxial tests over a range of confining pressures in which the maximum stress ratio decreases (curved failure envelope) and the volumetric strain behavior gradually changes from expansive to compressive with increasing confining pressure. The post-peak behavior is also correctly modeled in the range of confining pressures employed in the tests. The predicted behavior for proportional loading with increasing stresses is compared with the measured behavior for one of the cohesionless soils in loose and dense states, and stresses as well as strains occurring under K_o-conditions can be calculated with good accuracy. Finally, the stress-strain and pore pressure behavior observed in undrained tests on both loose and dense sand are accurately predicted.

None of the aspects of soil behavior included in the previous theory have been sacrificed in the elasto-plastic theory presented here. The previous theory is merely a special case included in the modified theory, i.e. for straight failure envelopes the modified theory without the cap is similar to the previous theory. Therefore, the modified theory is applicable to general three-dimensional stress conditions, but the fourteen soil parameters required to characterize the soil behavior can be derived entirely from the results of isotropic compression and conventional drained triaxial compression tests.

Acknowledgements—The original test data for Sacramento River Sand were kindly provided by K. L. Lee of the University of California, Los Angeles. The research presented here was supported by the National Science Foundation under Engineering Research Initiation Grant No. GK 37445.

REFERENCES

1. P. V. Lade, The stress-strain and strength characteristics of cohesionless soils. Ph.D. Dissertation, University of California, Berkeley (1972).
2. P. V. Lade and J. M. Duncan, Elastoplastic stress-strain theory for cohesionless soil. *ASCE: J. Geotech. Eng. Div.* **101**, 1037 (1975).
3. P. V. Lade and J. M. Duncan, Cubical triaxial tests on cohesionless soil. *ASCE: J. Geotech. Eng. Div.* **99**, 793 (1973).
4. P. V. Lade and J. M. Duncan, Stress-path dependent behavior of cohesionless soil. *ASCE: J. Geotech. Eng. Div.* **102**, 51 (1976).
5. K. L. Lee and H. B. Seed, Drained strength characteristics of sands. *ASCE: J. Soil Mech. Found. Div.* **93**, 17 (1967).
6. M. M. Al-Hussaini, Drained plane strain and triaxial compression tests on crushed Napa basalt, USAE WES, Miss., Report S-71-2, No. 2, June 1971.
7. M. M. Al-Hussaini, Plane strain and triaxial compression tests on Painted Rock Dam material, USAE WES, Miss., Report S-71-2, No. 3, September 1972.
8. J. M. Duncan and C.-Y. Chang, Nonlinear analysis of stress and strain in soils. *ASCE: J. Soil Mech. Found. Div.* **96**, 1629 (1970).
9. I. Holubec, Elastic behavior of cohesionless soil. *ASCE: J. Soil Mech. Found Div.* **94**, 1215 (1968).
10. C. R. Calladine, Overconsolidated clay: A microstructural view. *Proc. Symp. Role of Plasticity in Soil Mechanics* (Edited by A. C. Palmer). p. 144. Cambridge University (1973).
11. D. C. Drucker, R. E. Gibson and D. J. Henkel, Soil mechanics and work-hardening theories of plasticity. *ASCE Trans.* **122**, 338 (1957).
12. K. H. Roscoe and J. B. Burland, On the generalized stress-strain behavior of "wet" clay. *Engineering Plasticity* (Edited by J. Heyman and F. A. Leckie), p. 535. Cambridge University (1968).
13. F. L. DiMaggio and I. S. Sandler, Material model for granular soils. *ASCE: J. Eng. Mech. Div.* **97**, 935 (1971).
14. J.-H. Prevost and K. Höeg, Effective stress-strain-strength model for soils. *ASCE: J. Geotech. Eng. Div.* **101**, 259 (1975).
15. D. C. Drucker, Some implications of work hardening and ideal plasticity. *Quart. Appl. Math.* **7**, 411 (1950).
16. D. C. Drucker, A more fundamental approach to stress-strain relations. *ASME: 1st Nat. Cong. Appl. Mech.*, p. 487 (1951).
17. R. Hill, *The Mathematical Theory of Plasticity.* Oxford University Press (1950).
18. M. L. Silver and H. B. Seed, Volume changes in sands during cyclic loading. *ASCE: J. Soil Mech. Found. Div.* **97**, 1171 (1971).
19. T. L. Youd, Compaction of sands by repeated shear straining. *ASCE: J. Soil Mech. found. Div.* **98**, 709 (1972).
20. H. B. Poorooshasb, I. Holubec and A. N. Sherbourne, Yielding and flow of sand in triaxial compression: Part I. *Can. Geotech. J.* **3**, 179 (1966).
21. H.-Y. Ko and R. F. Scott, Deformation of sand in shear. *ASCE: J. Soil Mech. Found. Div.* **93**, 283 (1967).
22. M. A. El-Sohby, Deformation of sands under constant stress ratios. *Proc. 7th Int. Conf. Soil Mech. Found. Eng.*, Mexico City, Vol. I, 111 (1969).
23. P. W. Rowe, Theoretical meaning and observed values of deformation parameters for soil. *Proc. Stress-Strain Behavior of Soils* (Edited by R. H. G. Parry), p. 143. Cambridge University (1971).
24. K. Z. Andrawes and M. A. El-Sohby, Factors affecting coefficient of earth pressure K_0. *ASCE: J. Soil Mech. Found. Div.* **99**, 527 (1973).
25. A. W. Bishop and D. J. Henkel, *The Measurement of Soil Properties in the Triaxial Test*, 2nd Edn. St. Martin's Press (1962).
26. A. J. Hendron, The behavior of sand in one-dimensional compression. Ph.D. Dissertation, University of Illinois, Urbana (1963).
27. E. W. Brooker and H. O. Ireland, Earth pressures at rest related to stress history. *Can. Geotech. J.* **2**, 1 (1965).
28. H. B. Seed and K. L. Lee, Undrained strength characteristics of cohesionless soils. *ASCE: J. Soil Mech. found. Div.* **93**, 333 (1967).